# Vacancy engineering in $MoS_2$ nanolayers coupled with dual-carbon confinement for potassium storage

Xiaotong Wei [a], Shuang Tian [a, *], Tengteng Wang [a], Jingyi Huang [a], Peibo Gao [a], Yu Feng [a], Guangchao Yin [a], Jin Zhou [b], Tong Zhou [a, *]

[a] *School of Physics and Optoelectronic Engineering, Shandong University of Technology, Zibo 255049, China*

[b] *School of Chemistry and Chemical Engineering, Shandong University of Technology, Zibo, 255049, China*

***Corresponding author.**

*E-mail addresses:* tianshuang@sdut.edu.cn (S. Tian), zhoutong@sdut.edu.cn (T. Zhou).

## Experiment Section

**Preparation of $MoS_2$@CNTs:** 0.484 g of sodium molybdate (99.0%, Aladdin Co., Ltd.) and 0.912 g of thiourea (≥99.0%, Aladdin Co., Ltd.) were dissolved in 30 mL of mixed solution (DMF: deionized water = 1:1) and stirred for 30 min. Then 80 mg of MWCNTs was added with continuous stirring for 2 h. The above solution was transferred to a 50 mL Teflon-lined autoclave and reacted at 200 °C for 24 h. After cooling down to room temperature, the obtained sample was washed repeatedly with deionized water and ethanol and freeze-dried for 12 h. The dried samples were placed in the middle of the tube furnace, and 0.3 g of monolithic sulfur was placed in the front of the quartz tube. And the samples were fully sulfurized under nitrogen atmosphere at 800 °C for 2 h with a heating rate of 5 °C $min^{-1}$ to obtain $MoS_2$@CNTs.

**Preparation of $MoS_{2-x}$@CNTs:** The $MoS_2$@CNTs samples were placed in the middle of the tube furnace and raised to 650 °C under Ar atmosphere at a heating rate of 5 °C $min^{-1}$, then the hydrogen (7% in argon) was passed and kept for 20 min to obtain $MoS_{2-x}$@CNTs.

**Preparation of C-$MoS_{2-x}$@CNTs:** The $MoS_{2-x}$@CNTs was dissolved in 100 mL of Tris-buffered solution (10 mM, pH 8.5). 200 mg of dopamine (98%, Aladdin Co., Ltd.) was added to the solution with stirring for 5 h to obtain PDA-coating $MoS_{2-x}$@CNTs. Then washed with deionized water for several times, and freeze-dried for 12 h. Finally, the PDA-coating $MoS_{2-x}$@CNTs was carbonized in tube furnace under Ar atmosphere at 600 °C for 3 h to obtain the C-$MoS_{2-x}$@CNTs.

**Material Characteristics:** The morphology and structure of samples were

characterized by field emission scanning electron microscope (FESEM, HITACHI, SU8010) and transmission electron microscope (TEM, FEI Tecnai G2 F20 S-TWIN). X-ray powder diffraction (XRD) patterns were recorded from Bruker D8 Advance powder X-ray diffractometer with Cu Ka (λ = 0.15406 nm). Raman spectra were collected from a LabRAM HR evolution spectrometer under the excitation 532 nm laser. X-ray photoelectron spectroscopy were carried out on a Thermo Scientific ESCALAB 250XI equipment with Al Kα as the excitation source. BET surface area and pore size distribution were evaluated by $N_2$ adsorption/desorption analyzer (ASAP 2420, Micrometrics). Thermogravimetric analysis (TGA) was performed using PerkinElmer TGA 4000 in the temperature range of 30-800 ℃ at a heating rate of 10 ℃ $min^{-1}$ in air.

**Electrochemical Measurement:** The working electrodes were fabricated by uniformly pasting electrode slurry onto cupper foil, in which the electrode slurry consists of active material (80 wt%), ketjen black (10 wt%), polyvinylidiene fluoride (PVDF, Atofina) (10 wt%) and N-methylpyrrolidone (NMP) solution. Then, the electrodes were dried at 80 ℃ under vacuum for more than 12 h. All electrodes with an areal density of about 1.0 mg $cm^{-2}$ were assembled into CR2032-type cells under Ar glove box ($H_2O$ and $O_2$ < 0.01 ppm, Mikrouna Super). The K foil was used as the counter electrode for the half-cell and 1.0 M KFSI in EC: DEC = 1:1 vol% was used as the electrolyte. Galvanostatic charge/discharge tests were performed with the Land CT2001A battery testing system. Cyclic voltammetry and electrochemical impedance spectroscopy were carried out on an electrochemical workstation (IVIUM technology, nSTAT). The current density and

the capacity are based on the total mass of the electrodes.

**GITT Measurement:** Measurements of GITT profiles were made with pulse current at 0.05 A $g^{-1}$ for 10 min between rest intervals for 20min. The diffusivity coefficient can be estimated according to Fick's second law as follows:

$$D_k^+ = \frac{4}{\pi\tau}\left(\frac{m_B V_M}{M_B S}\right)^2\left(\frac{\Delta E_S}{\Delta E_t}\right)^2$$

where $m_B$ and $M_B$ are the effective mass and molar mass of the electrode material, respectively. $V_M$ is the molar volume, $S$ is the surface area of the electrode, $\Delta E_S$ is the voltage change between the initial and steady state, $\Delta E_t$ is the constant current discharge/charge potential change.

**Fabrication of PIC full cell:** PIC devices were also assembled into CR2032-type cells. Before assembling the PIC full cell, the C-$MoS_{2-x}$@CNTs anode was pre-cycled five times at 0.05 A $g^{-1}$ in half cell. PICs full cell was assembled by the pre-activated C-$MoS_{2-x}$@CNTs and Active carbon with mass ratios of 1:1, 1:2 and 1:3.

In PIC full-cell tests, the specific capacities and current densities were all based on the total mass of both anode and cathode materials. The calculations of energy density (E, Wh $kg^{-1}$) and power densities (P, W $kg^{-1}$) were performed using the equations below:

$$E = \int_{t_1}^{t_2} IV dt = \Delta V \times \frac{1}{m} \times t \qquad P = \frac{E}{t}$$

where $\Delta V$ represents the potential change after full discharge, $I$ is the constant discharge current, and $m$ is the total mass of the anode and cathode materials, $t$ is the time for a full discharge.

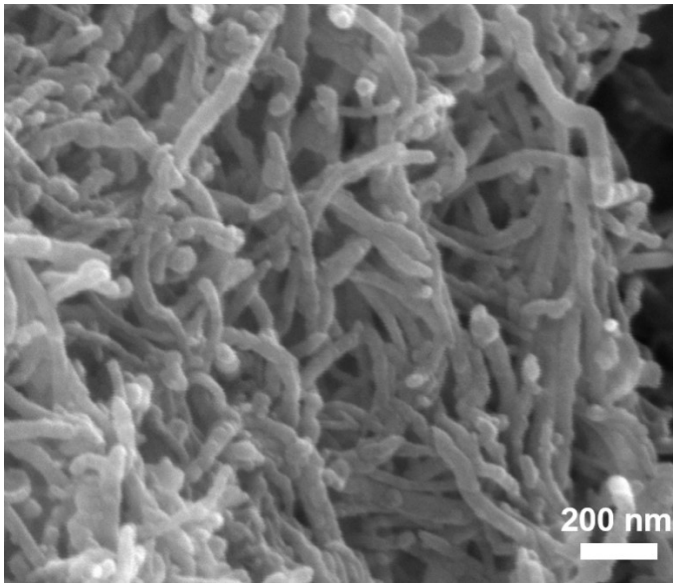


**Fig. S1** SEM image of the $MoS_2$@CNTs.

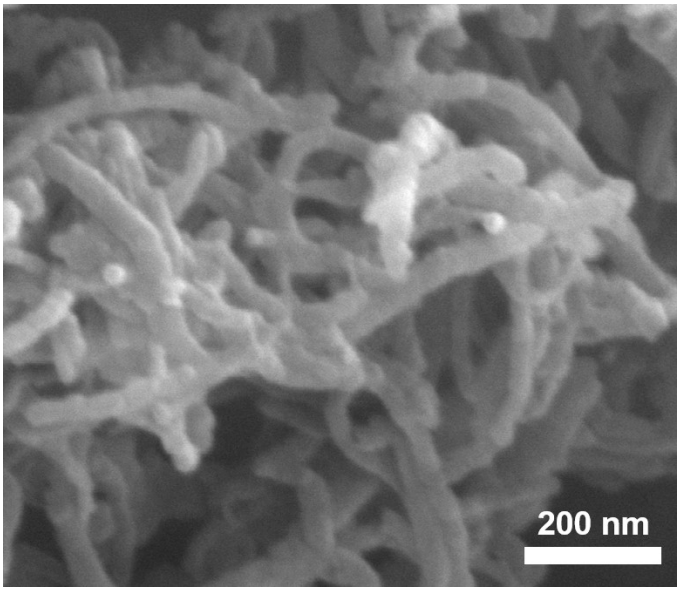


**Fig. S2** SEM image of the $MoS_{2-x}$@CNTs.

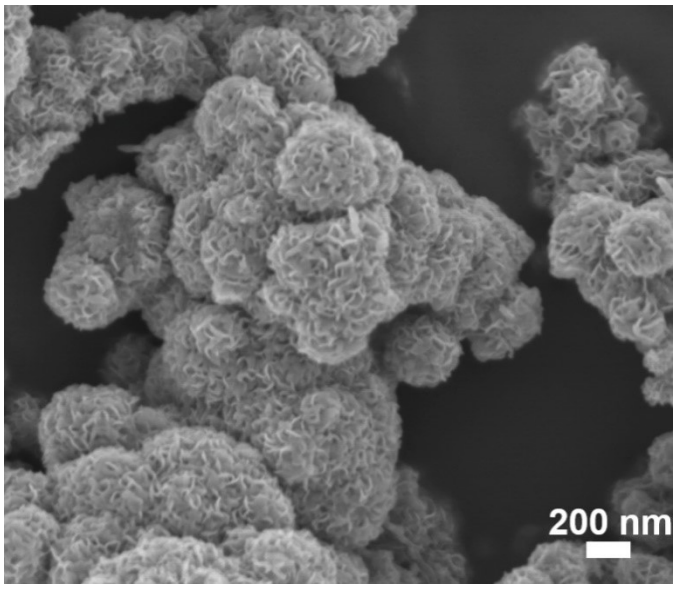


**Fig. S3** SEM image of the B-$MoS_2$.

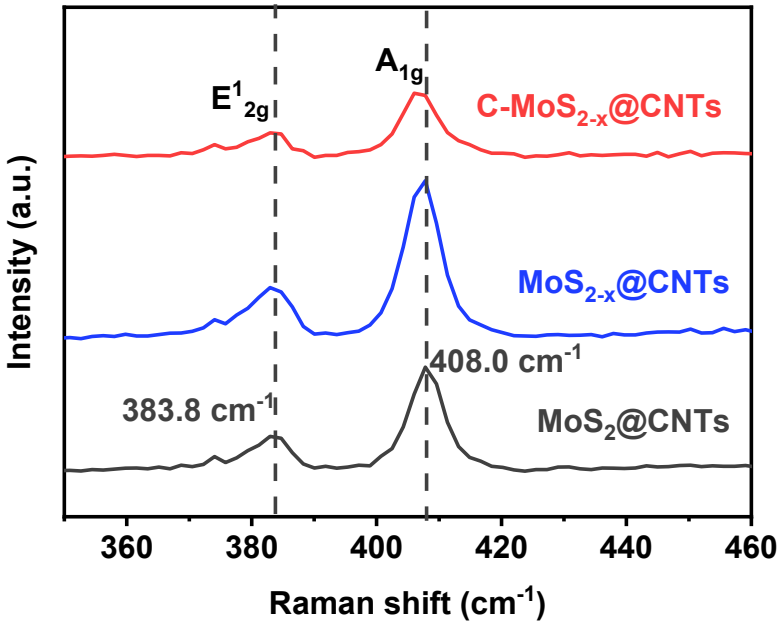


**Fig. S4** Regional enlargement of Raman spectra.

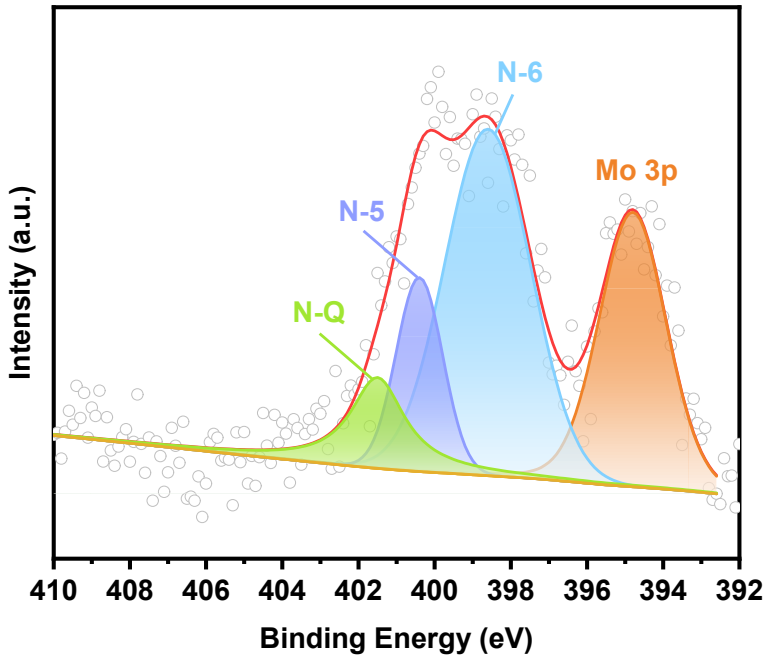


**Fig. S5** N 1s spectrum of C-$MoS_{2-x}$@CNTs.

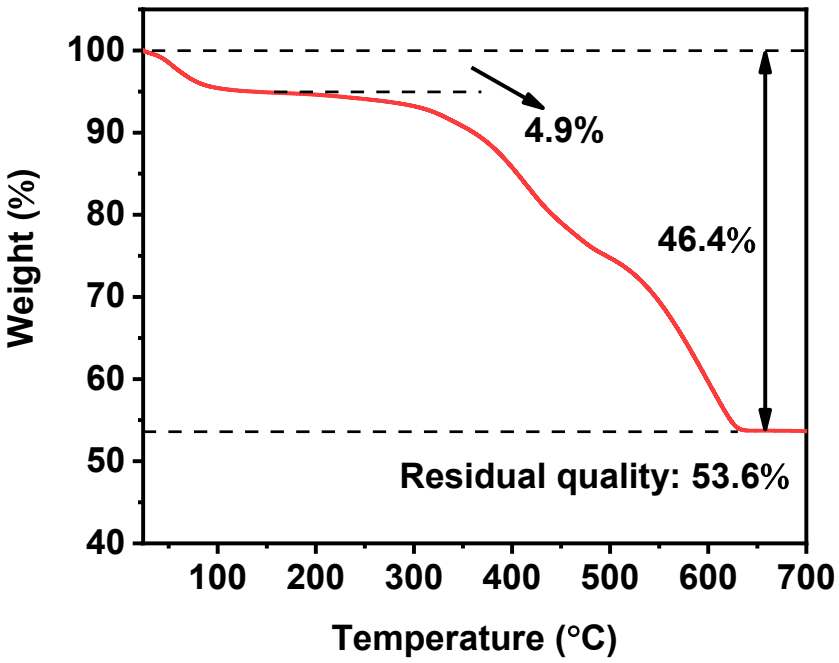


**Fig. S6** Thermogravimetric analysis of C-$MoS_{2-x}$@CNTs.

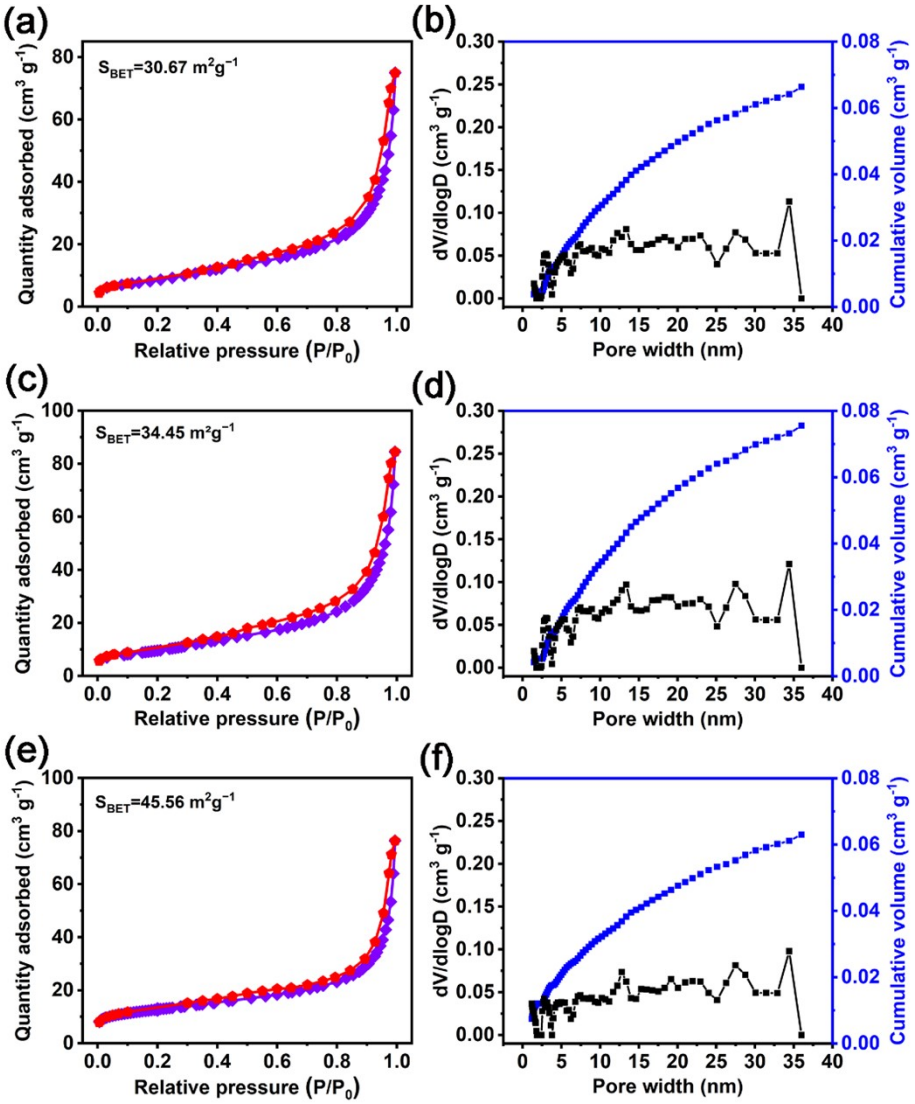


**Fig. S7** (a) $N_2$ adsorption-desorption isotherm, and (b) pore size distribution of the $MoS_2$@CNTs, (c, d) $MoS_{2-x}$@CNTs, and (e, f) C-$MoS_{2-x}$@CNTs.

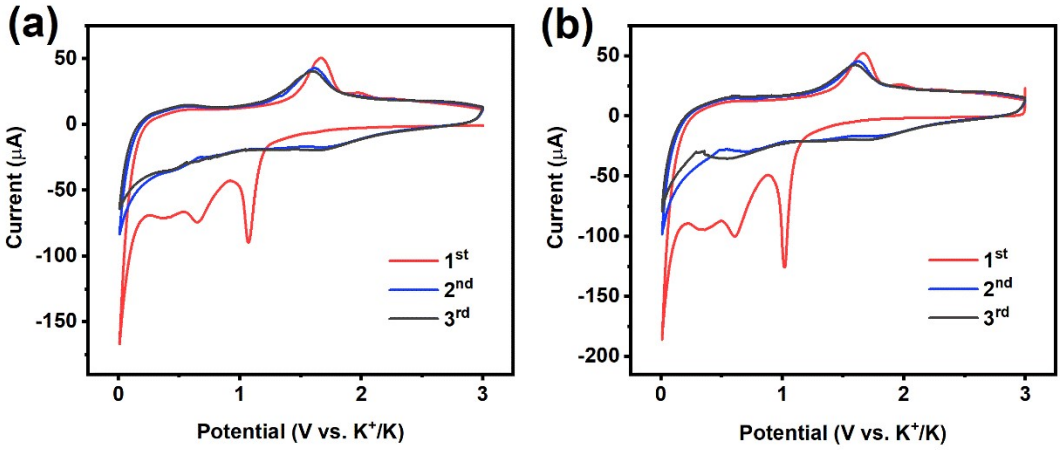


**Fig. S8** The initial three CV curves at 0.1 mV $s^{-1}$ of (a) $MoS_2$@CNTs, (b) $MoS_{2-x}$@CNTs.

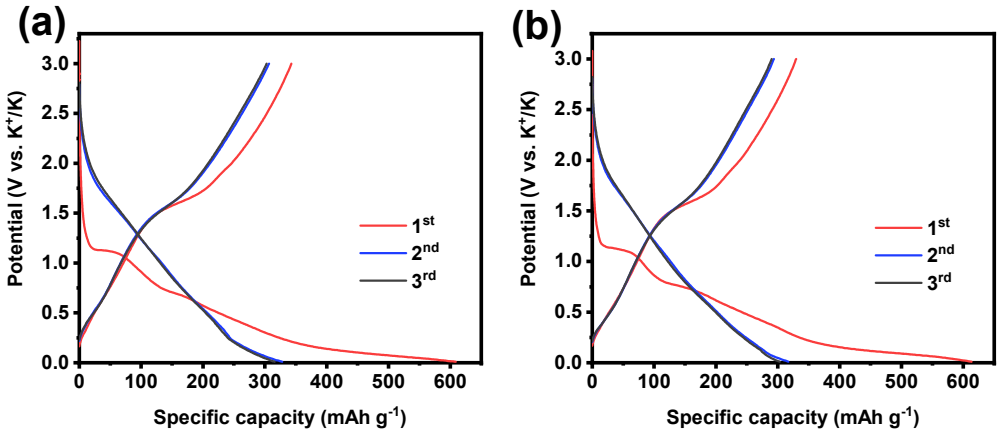


**Fig. S9** Discharge-charge profiles at 0.05 A $g^{-1}$ of (a) $MoS_2$@CNTs, (b) $MoS_{2-x}$@CNTs.

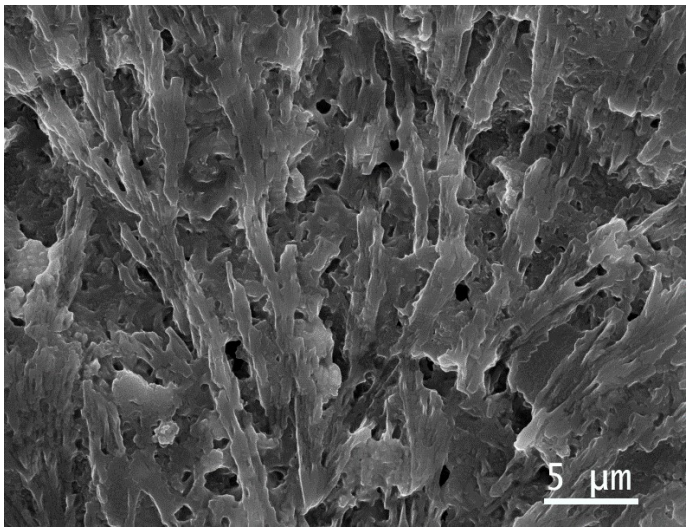


**Fig. S10** SEM image of C-$MoS_{2-x}$@CNTs after the cycling test

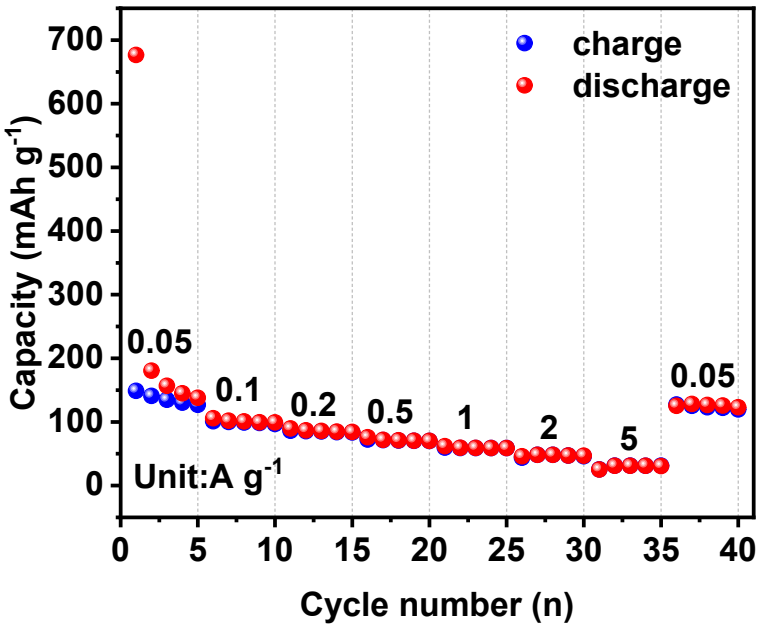


**Fig. S11** Rate capabilities of the CNTs.

**Table S1** Comparison of the electrochemical performance of C-$MoS_{2-x}$@CNTs anode with previously reported anode materials for PIBs.

| Anode materials | Rate capability | Reference |
|---|---|---|
| **C-$MoS_{2-x}$@CNTs** | **323.8mA h $g^{-1}$@0.05 A $g^{-1}$<br>180.9mAh $g^{-1}$@2 A $g^{-1}$** | **This work** |
| $S_v$-$WS_2$ | 303.3 mA h $g^{-1}$@0.05 A $g^{-1}$<br>136.6 mA h $g^{-1}$@2 A $g^{-1}$ | J. Power Sources. 542 (2022) 231791 |
| 2H-$MoS_2$/CNC | 220 mA h $g^{-1}$@0.05 A $g^{-1}$<br>139 mA h $g^{-1}$@1 A $g^{-1}$ | Small 17 (2021) 2102263 |
| $FeSe_2$/N-C | 277 mA h $g^{-1}$@0.1 A $g^{-1}$<br>155 mA h $g^{-1}$@2 A $g^{-1}$ | Adv. Energy Mater. 10 (2019) 1903277 |
| $FeSe_2$@C NBs | 257 mA h $g^{-1}$@0.1 A $g^{-1}$<br>128 mA h $g^{-1}$@1 A $g^{-1}$ | Chin. Chem. Lett. 32 (2021) 3601-3606 |
| $MoS_2$/N-doped-C | 258 mA h $g^{-1}$@0.1 A $g^{-1}$<br>131 mA h $g^{-1}$@2 A $g^{-1}$ | Adv. Funct. Mater. 28 (2018) 1803409 |
| $MoSe_2$/N-C | 300 mA h $g^{-1}$@0.1 A $g^{-1}$<br>178 mA h $g^{-1}$@2 A $g^{-1}$ | Adv. Energy Mater. 8 (2018) 1801477 |
| S-HCS | 389 mA h $g^{-1}$@0.1 A $g^{-1}$<br>110 mA h $g^{-1}$@5 A $g^{-1}$ | Adv. Mater. 31 (2019) 1900429 |
| $V_S$-$WS_2$-Se@1 NS | 363.9 mA h $g^{-1}$@0.05 A $g^{-1}$<br>154.2 mA h $g^{-1}$@2 A $g^{-1}$ | ACS Appl. Mater. Interfaces 14 (2022) 51994-52006 |
| C-p-$MoS_2$/CNT | 284 mA h $g^{-1}$@0.05 A $g^{-1}$<br>168 mA h $g^{-1}$@2 A $g^{-1}$ | Adv. Funct. Mater. 33 (2022) 2207548 |

**Table S2** Comparison of the C-$MoS_{2-x}$@CNTs||AC with previously reported PICs.

| PICs | Rate capability | Reference |
|---|---|---|
| **C-$MoS_{2-x}$@CNTs\|\|AC** | **89.2 Wh $kg^{-1}$@160.8 W $kg^{-1}$<br>60.2 Wh $kg^{-1}$@12.05 kW $kg^{-1}$** | **This work** |
| N-$MoSe_2$\|G\|\|AC | 119 Wh $kg^{-1}$@39.6 W $kg^{-1}$<br>29 Wh $kg^{-1}$@7212 W $kg^{-1}$ | Adv. Funct. Mater. 30 (2020) 1903878 |
| BSH | 120 Wh $kg^{-1}$@96 W $kg^{-1}$<br>13.3 Wh $kg^{-1}$@599 W $kg^{-1}$ | Adv. Mater. 30 (2018) 1800804 |
| $AgP_2$\|CNT\|\|AC | 37.3 Wh $kg^{-1}$@12.2073 kW $kg^{-1}$ | ACS Appl. Energy Mater. 6 (2023) 822-831 |
| HNTs@NG\|\|AC | 71.5 Wh $kg^{-1}$@214 W $kg^{-1}$ | Appl. Mater. Today 30 (2023) 101702 |
| S-KTO@C\|\|AC | 57.4 Wh $kg^{-1}$@1.74 kW $kg^{-1}$ | Small 16 (2019) 1906131 |
| $BiSbO_4$\|\|AC | 117.9 Wh $kg^{-1}$@100.5 W $kg^{-1}$<br>23.2 Wh $kg^{-1}$@3932.2 W $kg^{-1}$ | ACS Nano 16 (2022) 1486-1501 |